

**RESEARCH**

# Synthesis of Nano-Wall Like MnO<sub>2</sub> Electrode Material by Electrodeposition Method for Enhanced Capacitive Properties

S.S. Patil<sup>1,2</sup>, V.L. Patil<sup>2</sup>, A.K. Tawade<sup>3</sup>, K.K. Sharma<sup>3</sup>, T.D. Dongale<sup>3</sup>, R.M. Mane<sup>4</sup>, A.G. Bhosale<sup>1\*</sup>, S.A. Vanalakar<sup>2\*</sup>

<sup>1</sup>Department of Physics, Smt. Kusumtai Rajarambapu Patil Kanya Mahavidyalaya, Islampur, (Affiliated to Shivaji University, Kolhapur), Sangli 415409 (Maharashtra) India

<sup>2</sup>Department of Physics, Karmaveer Hire Arts, Science, Commerce and Education College, Gargoti, (Affiliated to Shivaji University, Kolhapur) Kolhapur 416209 (Maharashtra) India

<sup>3</sup>School of Nanoscience and Technology, Shivaji University Kolhapur 416004 (Maharashtra) India

<sup>4</sup>Department of Chemistry, Shivaji University, Kolhapur 416004 (Maharashtra) India

\*Corresponding authors:  
Email: sharad.vanalakar@gmail.com (S. A. Vanalakar)

agbkrpkmi@gmail.com (A. G. Bhosale)

## ABSTRACT

Supercapacitors are emerging as an alternative to batteries due to their high-power density, low charging time, safety, electrochemical stability, and long cycle life and manganese dioxide (MnO<sub>2</sub>) is one of the best electrode materials to prepare supercapacitor. In this regard, the MnO<sub>2</sub> as an electrode material was synthesized by using the simplistic electrodeposition method and various characterization techniques were carried out to investigate their physicochemical properties. The scanning electron microscopy illustrates the interconnected nano-wall like morphology of MnO<sub>2</sub> thin films, resulting in a larger surface area. This morphology is beneficial for providing more active sites for charge storage and hence leads to a higher capacitance. Therefore, the nano-wall like structure of MnO<sub>2</sub> thin films were utilized for the electrochemical measurements and it revealed higher specific capacitance at about 465 F/g for low scan rate of 10 mV/s. Furthermore, even after 500 cycles of voltammetry, the MnO<sub>2</sub>-based supercapacitor exhibits a higher cycling stability of about 98%.

## KEYWORDS

MnO<sub>2</sub> electrode, Nano-wall structure, Thin Film, Electrodeposition, Specific capacitance, Supercapacitor.

## INTRODUCTION

The rapidly growing human population, along with increased energy consumption, drives the scientific community to research novel energy-related technologies such as sources and storage systems [1]. In today's energy industry, the search for efficient and environmentally friendly energy sources and storage technologies presents considerable problems. Currently, we rely on fossil fuels at a pace of about 1 million barrels per day, despite their limited availability and significant contamination potential to generate energy [2]. Consequently, the energy research community is actively exploring alternate green energy sources. Along with energy generation, efficient storage is also an important factor in the energy industries. Now-a-days, the devices such as capacitors or supercapacitors, batteries, and fuel cells were utilized for storing electrical energy. Each device has their unique characteristics. Supercapacitors, for example, provide high power but low energy density, making them efficient energy storage

devices that fall somewhere between batteries and normal capacitors in terms of features. Recently, attention has been focused on developing advanced electrode materials to meet the requirements of supercapacitors for powering a wide range of portable electronic and consumer devices, including power sources, automobiles, camera, computers, hybrid vehicles, generators, inverters and even in bioelectronics [3].

Supercapacitors are often categorized into two types depending on their charge storage mechanism such as electric double layer capacitors (EDLCs) and pseudocapacitors. The EDLCs type of supercapacitors progressively store charges via a non-faradic reaction. In EDLCs, the electrical phenomena that develop at the interface between the conductive electrode and liquid electrolyte help to store the electrical charges. On the other hand, in the pseudocapacitors, the charge stores electrochemically, getting energy via faradic redox reactions [4]. There is another category known as hybrid capacitor devices which is combination of both EDLCs

and pseudocapacitors. Recently, various transition metal oxides such as  $\text{RuO}_2$ ,  $\text{Fe}_2\text{O}_3$ ,  $\text{Co}_3\text{O}_4$ ,  $\text{V}_x\text{O}_y$ ,  $\text{NiO}$ , and  $\text{MnO}_2$  have been widely used as electrode materials in hybrid devices due to their high electrochemical activity and variable oxidation state [4-6]. Out of which,  $\text{MnO}_2$  is one of the most promising electrode materials due to its earth abundance and environmental compatibility. About 20 years ago, Goodenough *et al.* revealed the Faradic pseudocapacitive behavior of micro  $\text{MnO}_2$  electrode material [7], and thereafter Miller *et al.* reported its highest theoretical specific capacitance of about 1370 F/g [8]. Furthermore, scientists have attempted to increase the capacitance of  $\text{MnO}_2$  material by manipulating particle size and shape via nanoparticle synthesis [9]. Meanwhile,  $\text{MnO}_2$  is prepared using a variety of processes, including hydrothermal [10], sol-gel [11], electrodeposition [12], chemical bath deposition [13], SILAR [14], and laser ablation [15]. However, the literature demonstrates that the specific capacitance of the  $\text{MnO}_2$  thin film depends on the pore size and surface shape [16-18]. Therefore, we have decided to use chemical methods to engineer the surface morphology of  $\text{MnO}_2$ . In the evaluation of chemical methods, electrodeposition method is more advantageous and affordable techniques in industrial processes that can result in the uniform films [19,20].

In present work, the electrodeposition technique was used to prepare  $\text{MnO}_2$  thin films, and its electrochemical properties were investigated. Furthermore, different characterization techniques were used to investigate the structural, morphological, and electrochemical features of the synthesized  $\text{MnO}_2$  thin films. The electrochemical performance of the  $\text{MnO}_2$  electrode material was assessed using cyclic voltammetry (CV), galvanostatic charge-discharge (GCD) analysis, electrochemical impedance spectroscopy (EIS), and longevity tests.

## EXPERIMENTAL DETAILS

### Preparation of $\text{MnO}_2$ thin films by using electrodeposition method

The  $\text{MnO}_2$  thin films were prepared using potentiodynamics electrodeposition method. The chemicals required for the preparation such as manganese sulphate ( $\text{MnSO}_4 \cdot \text{H}_2\text{O}$ ), sodium hydroxide ( $\text{NaOH}$ ) was purchased from S. D. Fine Chemicals, Mumbai (India) and used as received. During the experimental procedure, 0.1 M concentration solution of  $\text{MnSO}_4$  was prepared by dissolving  $\text{MnSO}_4$  in double distilled water. Then the pH of the solution was maintained at about 6.5 by adding 1M  $\text{NaOH}$  solution. This solution is used as electrolyte to deposit  $\text{MnO}_2$  thin films. The deposition was carried on the stainless steel (SS) substrates. Prior to deposition, the SS substrates were ultrasonically cleaned using double distilled water and acetone after being mirror polished with zero grade paper.

In a three-electrode electrochemical cell setup, the graphite was utilized as a counter electrode, saturated

calomel electrode (SCE) as a reference electrode, and stainless steel as the working electrode for the potentiodynamics electrodeposition method. All these electrodes were immersed in the prepared electrolyte solution. The deposition potential window was maintained from 0 to 1 Volt vs SCE. Since the electrodeposition scan rate has a major impact on the physico-chemical properties of the thin films, therefore, we have decided to study the effect of scan rates on  $\text{MnO}_2$  thin films. To make  $\text{MnO}_2$  thin films, a range of scan rates 10, 25, 50, and 100 mV/s was chosen and corresponding films were given the designations S1, S2, S3, and S4, respectively. In post deposition treatment, the deposited films were rinsed with double distilled water and then air dried at room temperature.

### Physicochemical Characterization

The structural analysis of as-synthesized  $\text{MnO}_2$  thin film was studied by using X-ray diffractometer (XRD) (Bruker D2 phaser, copper target  $\lambda=1.5404 \text{ \AA}$ ). The diffraction pattern was recorded within range of  $2\theta$  angles in between  $10^\circ$  to  $80^\circ$ . The surface morphologies of  $\text{MnO}_2$  thin films were characterized by Scanning Electron Microscopy (SEM) (JEOL JSM-IT200). Using SEM, high resolution images were captured at different magnifications.

### Electrochemical Measurements

The electrochemical behavior of  $\text{MnO}_2$  thin films were studied by using PC-controlled electrochemical analyzer (CH Instrument, USA, Model CHI-400A). All electrochemical measurements such as cyclic voltammetry (CV), galvanostatic charge-discharge (GCD) cyclic behavior and electrochemical impedance spectroscopy (EIS) were measured in 1M  $\text{Na}_2\text{SO}_4$  electrolyte solution using three electrode system. The three-electrode system include  $\text{MnO}_2$  thin film as the working electrode, platinum wire as the counter electrode and  $\text{Ag}/\text{AgCl}$  electrode as a reference electrode. The experimental setup used for electrochemical measurement is as shown in Fig. 1(a). The GCD tests were conducted by applying various constant current densities and recorded charge discharge curves. Thereafter, the specific capacitance was measured from the GCD curve. The surface and diffusion-controlled contribution is studied by using CV data.

## RESULT AND DISCUSSIONS

The thickness of  $\text{MnO}_2$  thin film on (1cm  $\times$  1cm) SS substrate was calculated by weight difference method, and it found the relative yield of  $\text{MnO}_2$  at about  $2 \times 10^{-4}$  gm. The XRD analysis was used to examine the structural properties of the as-synthesized  $\text{MnO}_2$  thin film deposited on the stainless-steel substrate and the resulting XRD pattern is displayed in Fig. 1(b). The XRD pattern showed a wide hump at the diffraction angle between  $20^\circ$  and  $25^\circ$ , but no clear diffraction peak. This demonstrates the amorphous nature of the as-deposited  $\text{MnO}_2$  thin films,

which are thought to be a good material for high-energy-density supercapacitor applications and may display pseudocapacitive behavior [21]. The SEM analysis was used to examine the surface morphology of the as-synthesized MnO<sub>2</sub> thin films, and the resulting SEM images of sample S1 are displayed in Fig. 1(c and d). The MnO<sub>2</sub> thin film's whole surface is covered with homogeneous, densely packed, highly porous, and linked nanosheets, as shown in the SEM images. The conduits of

a nanosize with several nano-walls are formed by the linked nanosheets. Walls have a diameter of around 10–30 nm and a length of 0.1–0.5 μm. Because of the intriguing, linked nano-wall structure formation, it exposes a larger effective surface area [22,23]. These provide access during the redox process, resulting in a high packing density of active material. Furthermore, the nano-sized material shortens the diffusion path of electron, which is advantageous in supercapacitor applications.

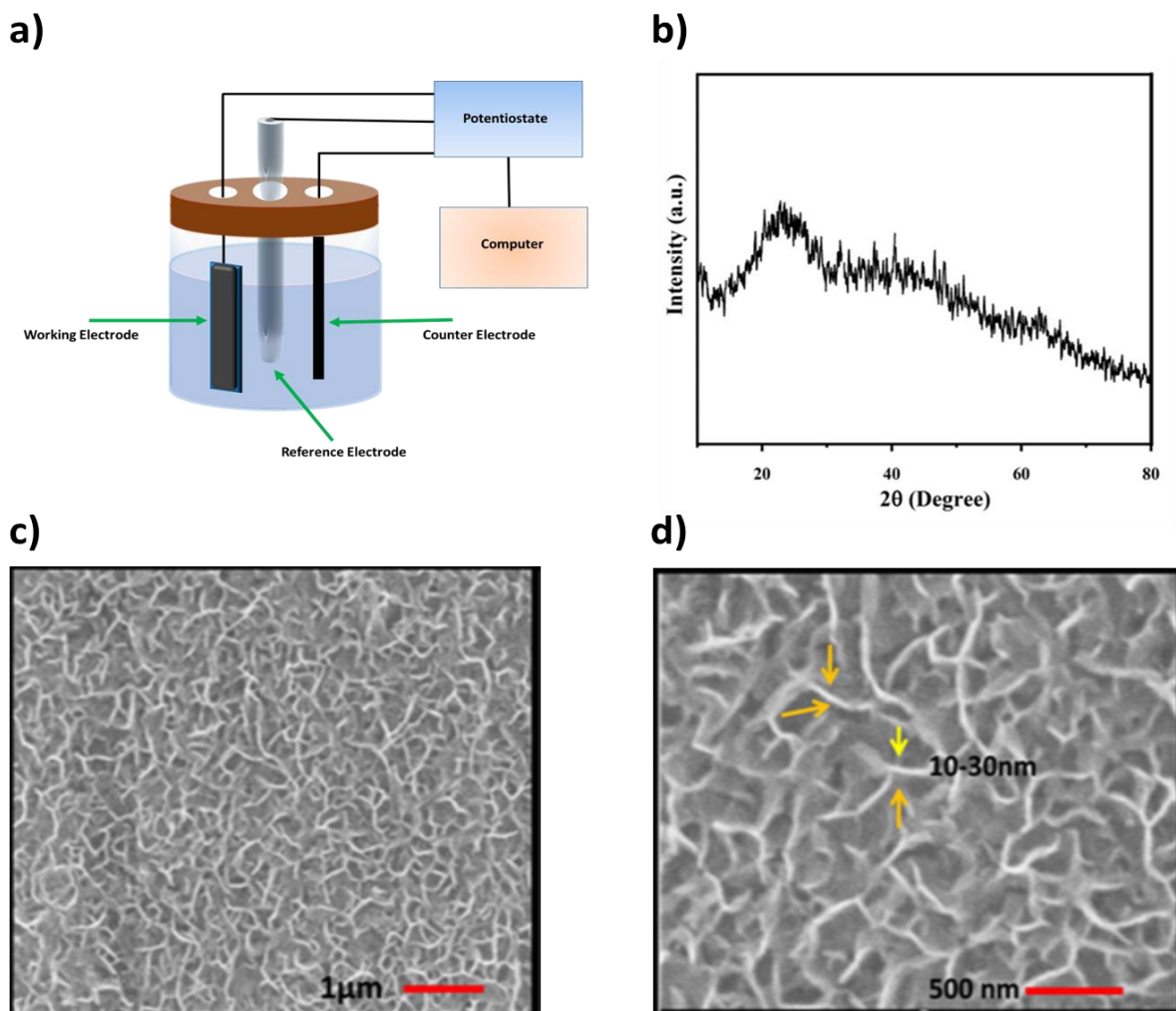


**Fig. 1.** (a) Schematic representation of electrodeposition set-up. The structural and surface morphological properties of MnO<sub>2</sub> thin film sample S1 including (b) XRD patterns (c) low magnification SEM image, and (d) high magnification SEM image showing the interconnected nanowires.

Furthermore, as synthesized MnO<sub>2</sub> thin films were used in capacitive charge storage applications. There are two types of capacitive charge storage mechanisms in MnO<sub>2</sub> electrodes: intercalation of alkali metal ions like Na<sup>+</sup> during reduction and de-intercalation during oxidation [24]. Equation (1) illustrates a possible reaction process.



The second type of capacitive charge storage process involves the adsorption/de-adsorption of alkali metals

(here Na<sup>+</sup> ions), on the surface of the MnO<sub>2</sub> nanostructure [25].



However, in the capacitive charge storage mechanism, the surface adsorption/desorption process is predominant in amorphous MnO<sub>2</sub> electrode material. In addition, the peculiar surface morphology plays a vital role during the adsorption and/or desorption processes.

The EIS provides a more comprehensive knowledge of the reaction kinetics for MnO<sub>2</sub> thin films; hence, EIS was used to characterize the electrodeposited interconnected nanowall like MnO<sub>2</sub> thin films using an electrolyte of 1M Na<sub>2</sub>SO<sub>4</sub>. **Fig. 2** depicts the Nyquist plot of all MnO<sub>2</sub> electrode samples such as S1, S2, S3 and S4. The semicircle indicated charge transfer impedance and minimal solution resistance. At lower frequency region, all these samples show inclined line which indicate ion diffusion processes within porous nano-walled like MnO<sub>2</sub> electrode material [26]. In this case, the EIS analysis supports the surface adsorption/desorption process in the capacitive charge storage mechanism. The values of electrolyte resistance (R<sub>s</sub>) for all MnO<sub>2</sub> samples are about 1.5 Ω, however, the charge transfer resistance (R<sub>ct</sub>) for sample S1, S2, S3 and S4 is about 180, 200, 250 and 350 Ω respectively. This suggests the variation in the kinetics of charge transfer process [27].

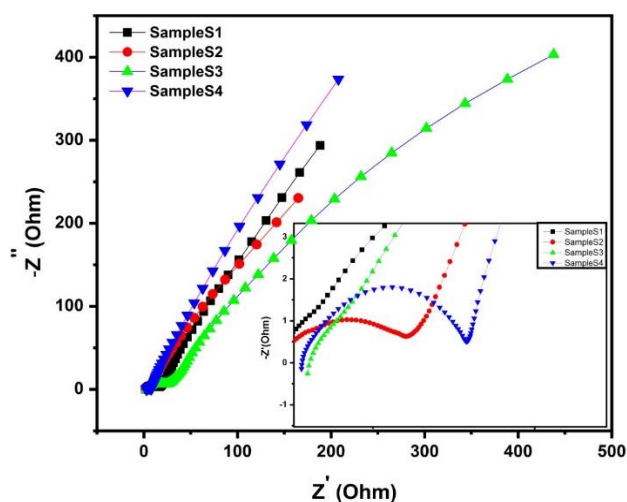


**Fig. 2.** EIS measurements of MnO<sub>2</sub> thin films samples S1, S2, S3 and S4.

Further, the electrochemical properties of nano-wall like MnO<sub>2</sub> based electrodes were studied by using the CV and GCD techniques. The CV is a well-known electrochemical technique to investigate the reduction and oxidation processes in the capacitive charge storage system. Here, all MnO<sub>2</sub> thin film samples were tested in three electrode systems to study the electron transfer-initiated chemical reactions. **Fig. 3(a)** reveals the CV graphs of all MnO<sub>2</sub> thin film samples in the voltage window of 0 to 1 V/SCE at 10 mV/s scan rate in 1M Na<sub>2</sub>SO<sub>4</sub> electrolyte. The specific capacitance (C<sub>sp</sub>) of MnO<sub>2</sub> thin films was estimated by the following equation

$$C_{sp} = \frac{\int I dv}{2vm} \quad (3)$$

where, m is the mass of the material, v is the scan rate and  $\int I dv$  is total average charge. The calculated values of specific capacitance as a function of MnO<sub>2</sub> samples were depicted in **Fig. 3(b)**. There is decrement in the specific capacitance for sample S1 to S4. The sample S1 shows the

higher specific capacitance as compared to other samples, therefore, we have decided to choose sample S1 for the further study.

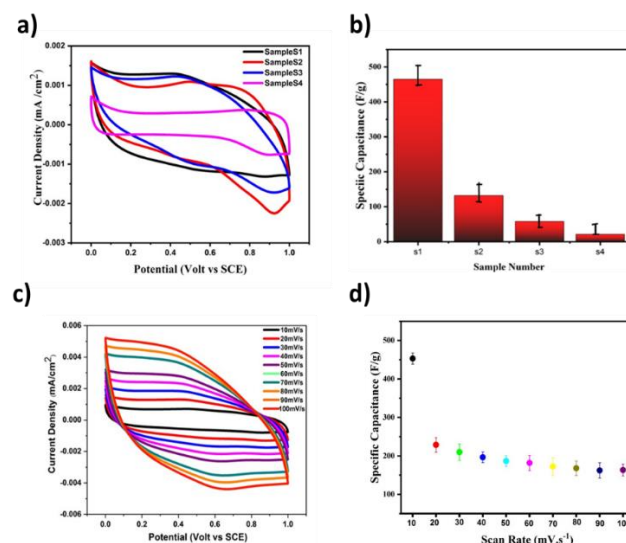


**Fig. 3.** Electrochemical properties of MnO<sub>2</sub> thin films including (a) CV curve of all MnO<sub>2</sub> samples recorded at the scan rate of 10 mV/s, (b) the plot of specific capacitance vs. MnO<sub>2</sub> samples S1, S2, S3 and S4, (c) CV curves of MnO<sub>2</sub> electrode sample S1 at the different scan rate ranging from 10 to 100 mV/s and (d) the plot of specific capacitance of MnO<sub>2</sub> electrode sample S1 against the scan rate.

**Fig. 3(c)** shows the CV of sample S1 at different scan rates ranging from 10 to 100 mV/s in 1M Na<sub>2</sub>SO<sub>4</sub> electrolyte. There is variation in the capacitance with respect to the scan rate. Interestingly the area under the curve at different scan rate is changes dramatically. However, the shape of the curve remains almost similar. The shape of CV curve is nearly quasi rectangular which is the characteristics of the pseudocapacitive nature. Meanwhile, **Fig. 3(d)** shows the values of specific capacitance as a function of scan rate for the sample S1. The higher specific capacitance of 465 F/g is observed at lower scan rate of 10 mV/s for sample S1, and it is higher than the recent report found in the literature [28-30]. The potential cause of drop of the specific capacitance at higher scan rates might be the electrolyte's resistance to the MnO<sub>2</sub> thin film's active surface area interaction. Since, at lower scan rate the ions in the electrolyte solution have sufficient time to fully diffuse into the porous structure of the nano-wall structure of MnO<sub>2</sub> electrode material. So, the maximum number of active sites can participate in the charge storage process, resulting in the high capacitance at a lower scan rate of 10 mV/s.

To study the contribution of capacitive reactions as well as Faradaic reactions in the MnO<sub>2</sub> sample S1, we have analyzed CV curves with the help of following equation.

$$i = i_{surface} + i_{diffusion} = av^b \quad (4)$$

where,  $i$  is peak current,  $v$  is scan rate and  $a$  and  $b$  are constants. To comprehend the dominating-controlled phenomenon, we computed the value of parameter  $b$  and plotted  $\log i$  vs  $\log v$  (Fig. 4(a)). In the meanwhile, the controlled phenomena are determined by the value of parameter  $b$ , which is recognized as a limitation of the charge storage mechanism. The charge storage process is caused by surface-controlled phenomena if parameter  $b$  has a value of 1, and diffusion-controlled phenomena if parameter  $b$  has a value of 0.5. The value of parameter  $b$  in our case is determined to be 0.99, which is quite near to 1, indicating that surface-controlled phenomena is dominant [31]. Additionally, the following equation was used to quantify the contributions of the diffusion-controlled and capacitive processes in the charge storage mechanism.

$$i(V) = kv + k'v^{\frac{1}{2}} \quad (5)$$

where,  $I$  denote current at the fixed potential  $V$ ,  $K$  and  $K'$  are two constants, and  $v$  is the scan rate. The contribution of current applied at various scan rates during the measurement of CV curves is displayed in Fig. 4(c). At every scan rate, the capacitive current contribution exceeds 80%, reaching around 97% at a scan rate of 100 mV/s. This suggests that the charge storage mechanism is mostly influenced by capacitive-controlled consequences. Because there is not enough time for ion migration into the lattice, the redox intercalation contribution decreases as the scan rate rises. Meanwhile, Fig. 4(b) shows the linear relationship of anodic/cathodic peaks at different scan rates ranging from 10 to 100 mV/s.

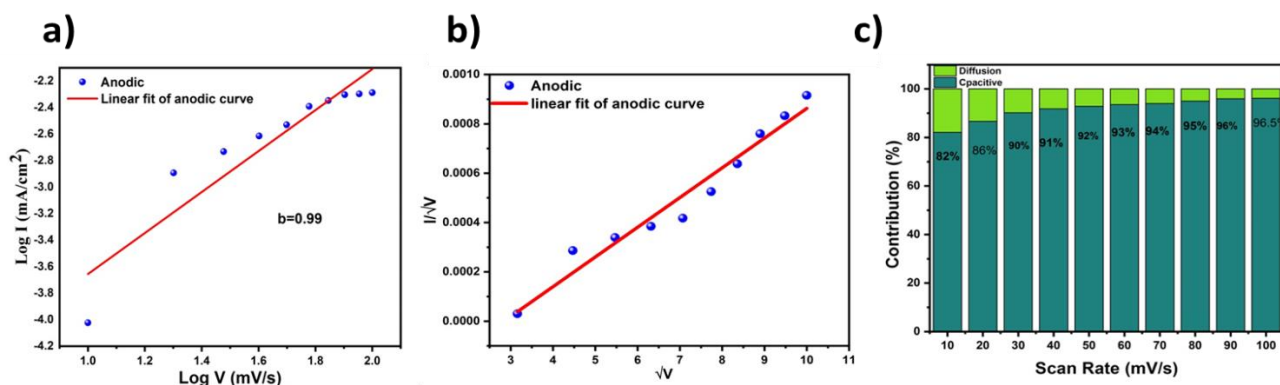


Fig. 4: (a) Plot of  $\log I$  vs.  $\log V$ , (b) linear relationship of anodic/cathodic peaks at different scan rates (10–100 mV/s), and (c) contribution of capacitive and diffusion-controlled phenomena in the charge storage mechanism.

In general, the GCD approach is utilized in addition to the CV to investigate the electrochemical performance of the supercapacitor electrode. Four samples, S1 through S4, have their GCD analyses examined; the results of each analysis are shown in Fig. 5(a) at a constant current density of 1 mA/cm<sup>2</sup>. It is evident that curves are not always perfect straight lines; instead, they frequently have a sawtooth appearance. Furthermore, the initial potential drop that corresponds with the electrode's internal resistance is also visible. The specific capacitance ( $C_s$ ) of an electrode in Na<sub>2</sub>SO<sub>4</sub> electrolyte is determined using the GCD curve, and for samples S1, S2, S3, and S4, it is about 284, 103, 51, and 20 F/g at a current density of 1 mA/cm<sup>2</sup> Fig. 5(b). Like CV measurements, there is a tendency of declining  $C_s$  for samples S2, S3, and S4 when compared to sample S1. Moreover, Fig. 5(c) illustrates the impact of current densities of 1, 2, and 3 mA/cm<sup>2</sup> on capacitance of sample S1. Meanwhile, higher current densities were associated with a sharper sawtooth-like form of the GCD, whereas lower current densities were associated with shorter charging and discharging times. For sample S1, the variation in specific capacitance in relation to the current density is depicted in Fig. 5(d). At around 1 mA/cm<sup>2</sup> of current density, the greater capacitance was seen. In

addition, our MnO<sub>2</sub>-based capacitor exhibits better capacitive performance when compared to other metal oxides including tin oxide and graphene oxide [32,33].

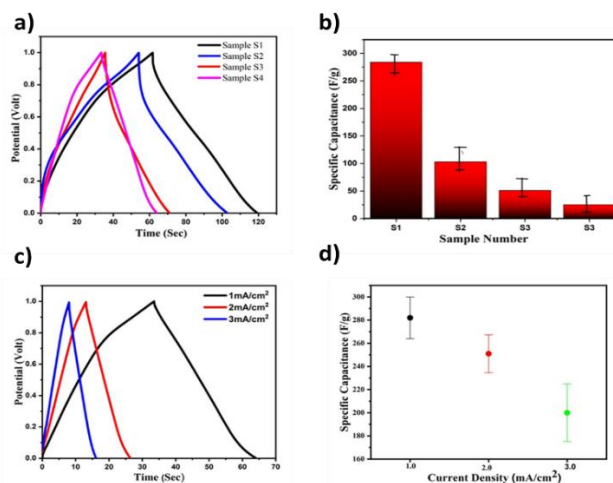


Fig. 5. (a) Galvanostatic charge-discharge (GCD) curves of sample S1, S2, S3 and S4 at current density 1 mA/cm<sup>2</sup>, (b) the plot of specific capacitance against the different MnO<sub>2</sub> thin film samples, (c) GCD of sample S1 at current density 1 to 3 mA/cm<sup>2</sup> and (d) the plot of specific capacitance calculated from GCD against current density.

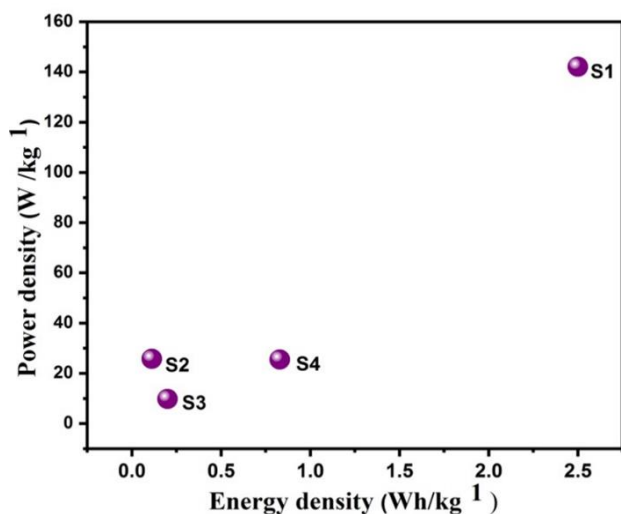


Fig. 6. Variation of energy density against power density for all MnO<sub>2</sub> thin film samples S1, S2, S3, and S4.

The energy and power density along with the capacity retention are other important criterion for the supercapacitive characterization of the electrode material. As a result, Fig. 6 displays the energy and power density of each MnO<sub>2</sub> thin film sample that was computed. The MnO<sub>2</sub> sample S1 exhibits a better power density of 2.5 W/kg and an energy density of around 142 Wh/kg. Meanwhile, a system's capacity retention refers to its ability to maintain stored energy over an extended period of open-circuit break time [34]. Even though it is dependent on the temperature, rest duration, and cell age, it is a crucial component of supercapacitors [35,36]. The capacitive retention of MnO<sub>2</sub> thin film sample S1 against cycle numbers is displayed in Fig. 7(a). Approximately 98% of the sample S1's capacitance is retained even after 500 continuous cycles. The excellent cycling ability of MnO<sub>2</sub> thin films is seen in Fig. 7. Here, the ratio of the first and last cycles (during the CV process) based capacitance is used to calculate the capacitance retention from gravimetric capacitance. After 500 cycles, there is a little decrease in the capacitance retention of our MnO<sub>2</sub> based supercapacitor device. The electrolyte or the forced redox reaction of the electrode with the electrolyte may be the cause behind the slight decrement in the capacitive retention. In the meantime, we have determined the MnO<sub>2</sub>-based supercapacitor's life cycle in the specified electrolyte. The life cycle analysis of sample S1 in 1M Na<sub>2</sub>SO<sub>4</sub> over 500 cycles, with a potential window of 0 to 1 V and a scan rate of 10 mV/s, is displayed in Fig. 7(b). As compared to the specific capacitance calculated for first cycle, the capacitance after 500 cycles is slightly decreased. As capacitive retention, the life cycle also highlighted the stability of as synthesized MnO<sub>2</sub> thin films. Overall, we have fabricated a stable and efficient MnO<sub>2</sub> based supercapacitor via simplistic electrodeposition technique.

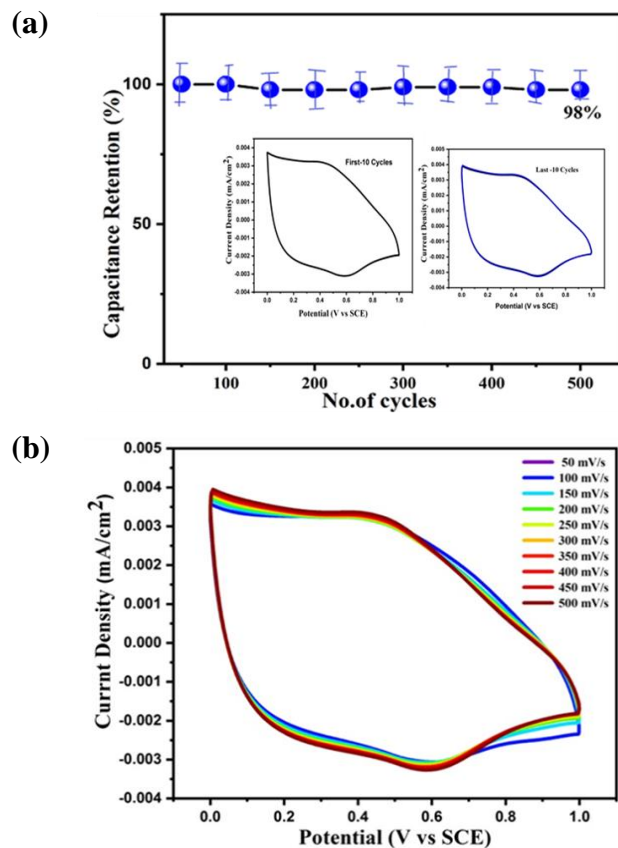


Fig. 7. (a) The stability study via capacitance retention of the sample S1 and (b) life cycles of sample S1 at different scan rate. Inset in Fig. 7 (a) shows the overlap CV of first 10 and last 10 cycles.

## CONCLUSION

We successfully developed a stable, porous, and efficient MnO<sub>2</sub> electrode in thin film form using a simple electrodeposition approach. The scanning electron microscopy revealed the extremely linked nano-wall like structure of the MnO<sub>2</sub> thin films. This connector assembly constructs nano-sized conduits, providing a larger surface area for electrolyte interaction in the capacitor device. The supercapacitive characteristics of nanostructured thin films of MnO<sub>2</sub> were investigated by using 1M Na<sub>2</sub>SO<sub>4</sub> as an electrolyte in a three-electrode setup and it found that the scan rate has a significant influence on the specific capacitance of MnO<sub>2</sub> films. The cyclic voltammetry measurements revealed a maximum specific capacitance of approximately 465 F/g at a lower scan rate of 10 mV/s, and even after 500 cycles, the MnO<sub>2</sub>-based supercapacitor maintained a cycling stability of around 98%. Thus, interconnected nano-wall like MnO<sub>2</sub> electrode in thin film form show maximum specific capacitance and 98% cycling stability. Such a specific feature indicates full potential of the MnO<sub>2</sub> electrode material, which provide an accurate measure of its intrinsic capacitance properties and promising performance for a highly efficient and durable energy storage devices.

## ACKNOWLEDGEMENTS

The author, SSP, would like to thank the Department of Physics at Smt. K.R.P. Kanya Mahavidyalaya Islampur, affiliated to Shivaji University Kolhapur, M.S. India, for providing research facilities, and the Chhatrapati Shahu Maharaj Research Training and Human Development Institute (SARTHII), Pune (Government of Maharashtra) for financial support under the Chhatrapati Shahu Maharaj National Research Fellowship-(CSMNRF-2021). This work is received funding from Shivaji University's Research Initiation Scheme 2020-21 (SU/C&U.D. Section/Prop. No. 101/1397) and Scientific and Technological Research Council of Turkey (Project No. 121C046).

## REFERENCES

1. Pruna A.L.; Lavered M. R.; Mataix D. B.; *Materials*, **2020**, 13, 624
2. Valdano P.; Esperance D.; Manguet N.; Mouana G.; *Statistical Review of World Energy*, **2020**, 9, 369-375
3. Kaya L.; Karatum O.; Balamur R.; Kaleli H. N.; Önal A.; Vanalakar S. A.; Hasanreisoglu M.; Nizamoglu S.; *Adv. Sci.*, **2023**, 10, 2301854
4. Zhou H.; Zou X.; Zhang Y.; *Inorg. Chem.*, **2019**, 58, 1591-1598.
5. Tarwate S. B.; Wahule S. S.; Gattu K.; Ghule A.V.; AIP Conf. Proc., 2018, 1953, 030052
6. Wang A. C.; Huang Y.; Xu Y.; Xu Y.; Jiao C.; Yuan L.; *CrystEngComm*, **2014**, 16, 385–392.
7. Goodenough. L.; Lee H.Y.; Goodenough J.B.; *J Solid State Chem*, **1999**, 144, 220-223.
8. Mille J. R.; Simon P.; *Mater Sci*, **2008**, 321, 651–652.
9. Jadhav P. R.; Suryawanshi M. P.; Dalavi D. S.; Patil D.S.; Jo E.A.; Kolekar S. S.; Wali A. A.; Karanjkar M .M.; Kim J. H.; Patil P. S.; *Electrochem Acta*, **2015**, 176,523-532.
10. Teli A. M.; Beknalkar S. A.; Pawar S. A.; Dubal D. P.; Dongale T. D.; *Energies*, **2020**, 13, 6124.
11. Khitams S.; Alyan, H; Alsalm A. d.; *Eng Tech J*, **2018**, 36 , 9.
12. Liu J.; Yang L.; Song Z.; Xu C.; *Appl Surf Sci*, **2019**, 478, 94-102.
13. Aref A. A.; Tang Y.; *Mater Sci Poland* **2014**, 4, 32.
14. Desai M.A.; Desai A.; Kulkarni A.; Gund G.; and Sarale S. D.; *Energy Fuels*, **2021**, 35, 4577-4586.
15. Zhange D.; Li Z.; Sugioka K.; *J. Phys. Photonics*, **2021**, 13, 042002.
16. Devaraj S.; Munichandraiah N.; *J. Phys. Che*, **2008**, 112, 4406-4417.
17. Devaraj S.; Munichandraiah N.; *Electrochem. Soc*, **2007**, 154, 80-88.
18. Pang S.C.; Anderson M. A.; Chapman T.W.; *J. Electron. Soc*, **2000**, 147, 444-450.
19. Wei W.; Cui X.; Chen W.; Ivey D. G.; *Chem. Soc. Rev*, **2011**, 40, 1697.
20. Gurav K.V.; Shin S.W.; Patil U.M.; Suryawanshi M.P.; Pawar S.M.; Gang M.G.; Vanalakar S.A.; Yun J.H.; Kim J.H.; *J. Alloys Comp*. **2015**, 631, 178–182.
21. Toupin M.; Brousse T.; Belanger D.; *Chem Mater*, **2004**, 16, 163-184.
22. Vanalakar S.A.; Mali S.S.; Pawar R.C.; Tarwal N.L.; Moholkar A.V.; Kim Jin. A.; Kwon Ye-bin; Kim J.H.; Patil P.S.; *Electrochimica Acta*, **2011**, 56, 2762-2768
23. Vanalakar S.A.; Mali S.S.; Jo E.A.; Kim J.Y.; Kim J.H.; Patil P.S.; *Solid State Sci.*, **2014**, 36, 41-46.
24. Zhao X.; Liu X.; Li F.; Huang M.; *Mater. Sci.*, **2020**, 6, 55.
25. Yang D.; Shu J.; You K.; Lin Z.G.; *J. Power Sources*, **1999**, 81, 637-641.
26. Jambhale P. M.; Narwade V.N.; Narwade V. N.; Shariq M.; Bogle K.; *J. Electron. Mater.*, **2024**, 6,10953.
27. Dhavale D. S.; Salunkhe R. R.; Dubal D. P.; Jamadade V.S.; Pawar S. M.; Lokhande C. D.; *Curr. Appl. Phys*, **2010**, 10, 904-909.
28. Wang He.; Wang H.; Hu C.; Cheng Y.; Yao L.; Ruan F.; Feng Q.; Chu C.; Lin T.; Wang H.; *J. Energ. Storage*, **2024**, 84, 110960.
29. Gang X. Li.; Wu Z.; Zhang J.Yao.; K Song.; S. Komarneni.; *Polymer*, **2024**, 292, 126623.
30. Deore K. B.; Narwade V. N.; Patil S. S.; Rondiya S. R.; Bogle K. A.; Tsai M-Lin.; Hianik T.; Shirsat M. D.; *J. Alloys Comp.*, **2023**, 958, 170412.
31. Tin Y.; Wang Q.; Peng Z.; Guan S.; Fu X.; *Molecules*, **2021**, 26, 4517.
32. Amade R.; Avetisyan A. M.; Gonzalez M.; depino A.P.; Gyorgy O.E.; Pascual E.; *Mater*, **2019**, 12, 483.
33. Barclay M.; Firestein K.; Wang X.; Motta N.; Dubal D.; Ostriko K.; *Mater. Today Sustainability*, **2023**, 22, 100388.
34. Kumar Y.; Chopra S.; Gupta A.; Kumar Y.; Uke S. J.; Mardikar S. P.; *Mater. Sci. Energ. Technolo*, **2020**, 3, 566-574.
35. Patil S.S.; Bhosale A.G.; Kundale S.S.; Dongale T. D.; Vanalakar S.A.; *Carbon Trends*, **2024**, 15, 100370.
36. Suhasini A.; Hegde C J.; *Electroanalytical Chem.*, **2012**, 676, 35-39.



This article is licensed under a Creative Commons Attribution 4.0 International License, which allows for use, sharing, adaptation, distribution, and reproduction in any medium or format, as long as appropriate credit is given to the original author(s) and the source, a link to the Creative Commons license is provided, and changes are indicated. Unless otherwise indicated in a credit line to the materials, the images or other third-party materials in this article are included in the article's Creative Commons license. If the materials are not covered by the Creative Commons license and your intended use is not permitted by statutory regulation or exceeds the permitted use, you must seek permission from the copyright holder directly.

Visit <http://creativecommons.org/licenses/by/4.0/> to view a copy of this license.